Bio-Design and Manufacturing (2025) 8:359–374
https://doi.org/10.1631/bdm.2400334

RESEARCH ARTICLE

Composite poly(lactic-co-glycolic acid) and a decellularized extracellular matrix conduit with Schwann cells for enhanced nerve regeneration

Zhifa Xue[1] · Yuye Huang[1,2] · De Bi[1,3] · Kai Ye[1,4] · Hangyu Zhou[1] · Lizhe He[2] · Peng Wei[1] · Yangjian Wang[1]

Received: 22 August 2024 / Accepted: 29 October 2024

Abstract

Peripheral nerve injuries (PNIs) affect approximately one million people globally every year. While autologous nerve transplantation remains the gold standard for healing PNIs with large gaps, limitations such as donor site morbidity and limited nerve availability present challenges in clinical application, highlighting the need for innovative solutions based on synthetic biomaterials. In this study, we explored a composite nerve conduit that combines a poly(lactic-co-glycolic acid) (PLGA) shell and a decellularized extracellular matrix (dECM) seeded with Schwann cells (SCs). In particular, the dECM, derived from rat sciatic nerves, retains the native tissue structure and bioactive components. In vitro studies showed that SC-seeded dECM promotes cell viability, proliferation, and alignment. In vivo testing using a rat sciatic nerve defect model demonstrated that the PLGA/dECM-SC conduit significantly improved nerve regeneration compared with conduits without SCs, showing enhanced axonal growth, myelination, and motor function restoration comparable to autografts. This approach offers a promising alternative to autologous nerve grafts in the clinical treatment of PNIs.

Graphical abstract

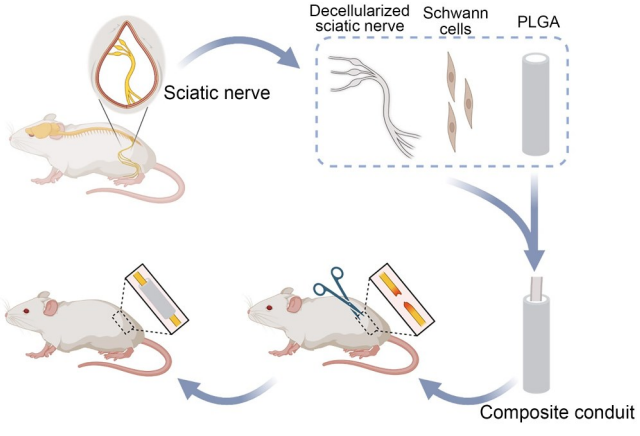

Keywords Peripheral nerve repair · Decellularized extracellular matrix (dECM) · Schwann cells · Neurotrophic factors

Zhifa Xue and Yuye Huang have contributed equally to this work.

✉ Peng Wei
weipeng@nbu.edu.cn

✉ Yangjian Wang
fyywangyangjian@nbu.edu.cn

[1] Department of Plastic and Reconstructive Surgery, The First Affiliated Hospital of Ningbo University, Ningbo 315010, China

[2] Center for Medical and Engineering Innovation, Central Laboratory, The First Affiliated Hospital of Ningbo University, Ningbo 315010, China

[3] Department of Neurosurgery, The First Affiliated Hospital of Ningbo University, Ningbo 315010, China

[4] The Second Affiliated Hospital, Zhejiang University School of Medicine, Hangzhou 310027, China

1 Introduction

Peripheral nerve injuries (PNIs) affect approximately one million people worldwide annually, imposing significant personal and societal burdens. While direct suturing of nerve ends is a viable therapeutic approach, its use is limited to injuries with short gaps (typically <10 mm) [1]. For larger gaps, autologous nerve transplantation remains the gold standard [2, 3]. However, this approach faces several challenges, including limited availability of appropriate donor nerves, discrepancies in lengths between donor nerves and injury sites, and post-transplant complications such as morbidity and impaired nerve function at the donor site [4]. These limitations highlight the urgent need for new therapeutic approaches that are both effective and widely applicable in clinical settings.

A promising alternative for PNI treatment is the implantation of nerve guidance conduits (NGCs) [5–7]. Based on tissue engineering principles, NGCs are tubular constructs that enclose severed nerve ends, promoting spontaneous regeneration and repair while protecting the injury site from invading fibrous tissue [8]. Ideally, NGCs should be fully degradable upon PNI healing; thus, they are fabricated using either natural biopolymers (e.g., collagen [9], chitosan [10], and silk fibroin [11]) or synthetic biodegradable polymers (e.g., poly(lactic-co-glycolic acid) (PLGA) [11] and polycaprolactone (PCL)) [12]. Once PNI characteristics (e.g., gap length, location, and presence of mechanical loading) and treatment goals (e.g., regeneration time and degradation rate) have been assessed, clinicians select an NGC with appropriate size and material composition for implantation [13]. However, a significant limitation of most NGCs in clinical use is their inability to actively stimulate nerve regeneration, often making them less effective than autologous nerve grafts. This challenge highlights the need for further research and development to enhance the regenerative capabilities of NGCs.

To enhance the regenerative capacity of NGCs, decellularized extracellular matrix (dECM) from nerves is increasingly being used as a bioactive substrate. Derived from native nerve tissue by removing cellular components, dECM retains numerous receptor recognition ligands and growth factors that promote cell adhesion and growth [14–16]. Despite its low mechanical strength, dECM has shown promise in creating an environment conducive to nerve regeneration [17]. However, since most viable cells and cytokines are removed during decellularization, dECM alone cannot consistently supply the biomolecules needed for sustained nerve regeneration, limiting its effectiveness in the later stages of PNI healing.

One strategy for enabling the long-term delivery of the biomolecules necessary for nerve regeneration is transplanting selected cells back into the dECM. These recolonized cells, capable of producing neurotrophic factors and other cytokines, ensure the sustained and localized delivery of functional biomolecules essential for effective PNI healing [18, 19]. Specifically, Schwann cells (SCs), native to the peripheral nervous system, have been widely applied due to their ability to support nerve regeneration and myelination following PNI [20, 21]. Studies have shown that decellularized rat SCs promote the survival of transplanted SCs, which in turn facilitate myelination and axonal growth, ultimately restoring motor function [22]. We propose that NGCs functionalized with dECM and SCs, compared to NGCs alone, more closely mimic the composition and structure of peripheral nerves, and are therefore expected to enhance nerve regeneration.

Our previous study demonstrated that PLGA conduits combined with decellularized rat nerves have significant potential for peripheral nerve regeneration; however, the lack of sustained cytokine delivery due to the absence of viable cells within the NGCs was considered a critical limitation [8]. In this study, we propose a composite nerve conduit in which the dECM from the sciatic nerve is first seeded with viable SCs and then sheathed in a PLGA conduit fabricated using the dry jet-wet spinning technique. The PLGA shell is expected to provide load-bearing capacity and prevent the invasion of undesired fibrous tissue, while the SC-seeded dECM serves as a biomimetic and bioactive substrate to enhance peripheral nerve regeneration. First, we examined the microstructure of the acellular sciatic nerve using scanning electron microscopy (SEM). Second, we assessed the biological function of the SC-seeded dECM through in vitro studies. Finally, we evaluated the therapeutic effect of the composite conduits in a classic rat sciatic nerve defect model, followed by histological and neurofunctional analyses. The results demonstrated that combining dECM and viable SCs contributed to restoring motor function, indicating a promising strategy for PNI treatment.

2 Materials and methods

2.1 Materials

PLGA was purchased from MedTech Instruments Co., Ltd. (Shandong, China). SCs were obtained from the Cell Bank of the Chinese Academy of Sciences (Shanghai, China), and the lentivirus of the negative control (green fluorescent protein (GFP)) was purchased from GenePharma (Jiangsu, China). Essential materials, such as Dulbecco's modified Eagle medium (DMEM), 0.25% trypsin-EDTA (ethylene diamine tetraacetic acid), 1% penicillin/streptomycin (P/S), and phosphate-buffered saline (PBS), were sourced from Gibco (Big Cabin, OK, USA). The TIANamp Genomic DNA Kit was purchased from Tiangen Biochemical Technology Co.

(Beijing, China), and the Cell Counting Kit-8 (CCK-8) reagent was purchased from Beyotime (Shanghai, China). Additional materials, including 3,3′-diaminobenzidine substrate solution, phalloidin-fluorescein isothiocyanate, hematoxylin and eosin (H&E), resin, 4′,6-diamidino-2-phenylindole (DAPI), and the Calcein-AM/propidium iodide (PI) kit (CA1630), were purchased from Solarbio (Beijing, China). The β-actin antibody (RM2001) was procured from Ray Antibody Biotech (Beijing, China), while the NF-H (ab207176), GAP-43 (ab16053), βIII-tubulin (ab18207), and S100β (ab52642) antibodies were obtained from Abcam (Cambridge, UK). The CD31 antibody (A0378) was purchased from Abclonal (Wuhan, China). Akt (4691), p-Akt (9271), p-PI3K (17366), and CD68 (97778) antibodies were purchased from Cell Signaling Technology (Boston, USA), and the PI3K antibody (20584-1-AP) was purchased from Proteintech (Wuhan, China). In addition, a bicinchoninic acid (BCA) protein assay kit (23225) was obtained from Thermo Scientific (Rockford, IL, USA). TRIzol and Power SYBR Green PCR Master Mix were obtained from Life and Vazyme, respectively (Waltham, MA, USA). All primers were synthesized by Sangon Biotech (Shanghai, China).

2.2 Preparation of decellularized rat peripheral nerves

Fresh sciatic nerves were collected from euthanized Sprague–Dawley (SD) rats housed at the Experimental Animal Center of Ningbo University. The excised nerves were washed thoroughly with PBS to remove residual blood, trimmed into about 1-cm segments, and placed in a 50-mL centrifuge tube filled with 2% Triton X-100 solution. This was followed by gentle shaking at room temperature for 24 h, with the solution refreshed after the first 12 h. The solution was then replaced with 0.1% sodium dodecyl sulfate (SDS), followed by 48 h of shaking, during which the solution was changed every 12 h. The nerve tissues were then transferred to deionized (DI) water and gently shaken for another 24 h, with water replacement done every 12 h. Finally, the decellularized peripheral nerve tissue samples were freeze-dried and stored at −20 °C until use.

2.3 Preparation of frozen tissue sections and SEM imaging

Coverslips (diameter: 12 mm) were pretreated by soaking in poly-L-lysine (PLL) solution (diluted 10-fold in sterile DI water) at room temperature for 5 min and then dried in an oven (BLUEPARD, DHG-9030, Shanghai, China) at 60 °C for 1 h. The decellularized nerve tissue was unfolded in a cryosection box with an area of about 0.2 cm^2, embedded in an optimal cutting temperature (OCT) compound (SAKURA, USA), and frozen at −20 °C for 1 h. The tissue was sliced into approximately 50-μm sections and placed on the pretreated coverslips for attachment. After air drying for 30 min, the OCT compound was carefully removed using fine forceps. The coverslips were then placed in a 24-well plate, washed sequentially with alcohol and PBS, and soaked in PBS for 12 h to remove any residual OCT compounds. Finally, the samples were sterilized under ultraviolet (UV) light for 60 min. The decellularized tissues were dehydrated and visualized using SEM (Phenom Pro, the Netherlands).

2.4 Mechanical testing of NGCs

The mechanical properties of the nerve conduits were investigated using a universal testing machine (AGS-X, Shimadzu, Japan). PLGA and PLGA/dECM conduits, each with a length of 20 mm, were secured in the device, with a 10-mm span between the grips. A constant tensile load at a rate of 2 mm/min was then applied. The nominal stress on the conduits was calculated based on their cross-sectional areas, as follows:

$$A_{\mathrm{PLGA}} = \pi DH,$$

$$A_{\mathrm{PLGA/dECM}} = \pi D^2/4.$$

Here, D is the outer diameter of the conduit (3.2 mm) and H is the wall thickness (0.15 mm). Nominal stress was calculated by dividing the applied load (in Newtons) by the calculated cross-sectional area. The tensile modulus was derived from the slope of the linear region within the 1%–2% strain range. Five replicates were tested for each group.

2.5 Cell culture

SCs (RSC 96) were purchased from the Cell Bank of the Chinese Academy of Sciences (Shanghai, China) and cultured in DMEM supplemented with 10% fetal bovine serum (FBS, Excell Bio, FCS500, USA) and 1% P/S. Cells were maintained up to 10 passages in a humidified incubator (Thermo Scientific, USA) at 37 °C with 5% CO_2. For cell seeding, coverslips with adhered decellularized nerve tissue were placed into 24-well plates, and 5×10^3 SCs dispersed in culture media were seeded directly onto the tissue sections. Cell proliferation was studied by visualizing the cells on different decellularized tissues under a light microscope on Days 1, 3, 5, and 7 after seeding.

2.6 Live/Dead assay

A fluorescence live/dead assay was conducted using the Calcein-AM/PI kit. Coverslips containing cells and decellularized nerves were washed three times with buffer, followed by incubation with 500 μL of working solution (2 μmol/L Calcein-AM and 4.5 μmol/L PI) for 15 min in a

humidified incubator. The stained samples were then washed three additional times with buffer before being visualized under a fluorescence microscope (DM2000; Leica, Wetzlar, Germany). The ratio of dead cells in the acquired images (n>3) was analyzed using ImageJ software (Version 1.53f51, National Institute of Health, USA).

2.7 Primary Schwann cell isolation and fabrication of the composite nerve conduit

Primary SCs were isolated from neonatal SD rats (1–3 d old) following a previously described protocol [23] and were cultured in DMEM supplemented with 10% FBS and 1% P/S. Lentivirus expressing GFP was used to infect the cells for 12 h, after which the medium was replaced with a complete culture medium for continued growth. Upon reaching 90% confluency, the SCs were seeded onto the dECM. After 24 h for cell attachment, a section of decellularized nerve tissue (about 1.2 cm) was placed into a PLGA conduit of the same length. One end of the decellularized tissue was sutured to the PLGA conduit using 9-0 microsutures, and the thread was then drawn through the opposite end of the conduit until the dECM was fully incorporated.

2.8 Acquisition and culture of neonatal DRGs

Under aseptic conditions, dorsal root ganglia (DRGs) were obtained from neonatal rat pups aged 3–7 d. Following anesthesia and disinfection, the spinal columns were removed to expose the DRGs, which were then trimmed, transferred to DMEM, and incubated at 37 °C with 5% CO_2. After 24 h, the DMEM was replaced with a specialized culture medium for an additional 5 d of in vitro culture. The DRGs and neuronal cells were subsequently subjected to immunofluorescence imaging. After fixation in 4% paraformaldehyde (PFA), the cells were permeabilized with 0.3% Triton X-100 and blocked with 5% bovine serum albumin (BSA). The cells were then incubated overnight at 4 °C with a βIII-tubulin primary antibody (1:200), followed by a donkey antimouse IgG secondary antibody for 1 h at room temperature. Finally, the samples were stained with DAPI for nuclei visualization and observed under a fluorescence microscope.

2.9 Functional assay of human umbilical vein endothelial cells (HUVECs)

To validate the effect of dECM-cultured SCs on endothelial cell migration, we conducted a Transwell migration assay. In brief, the experimental group used conditioned medium from SCs cultured on dECM, while the control group used conditioned medium from SCs cultured in blank wells. HUVEC suspensions (5×10^4 cells/mL) were placed in the upper Transwell chambers containing ECM medium, and the conditioned medium was added to the lower chambers. After 12 h of incubation, the number of migrated HUVECs was observed using crystal violet staining.

HUVECs were cultured in ECM medium supplemented with 10% FBS and seeded onto 24-well plates precoated with Matrigel (300 μL per well; BD Biosciences, State of New Jersey, USA). After 6 h of incubation in the conditioned medium at 37 °C, tube formation was observed and captured using an inverted microscope. The number of branch points in the connected tubes was quantified and compared between the groups.

2.10 Enzyme-linked immunosorbent assay (ELISA) for the secretion of neurotrophic factors

The secretion of β-nerve growth factor (β-NGF; R&D, USA), brain-derived neurotrophic factor (BDNF; Abcam, USA), and glial cell line-derived neurotrophic factor (GDNF; Abcam) from SCs on dECM was measured using ELISA based on the manufacturer's protocol. The supernatant of SC-laden dECM was collected on Day 7 and analyzed using a microplate reader (Molecular Devices, SpectraMax iD3, China).

2.11 Walking track analysis

At 16 weeks post-surgery, we stained the hind limbs of the rats with black ink and allowed them to walk through a wooden trough measuring 75 cm in length, 8 cm in width, and 15 cm in height. The footprints of the hind limbs were recorded on a piece of paper placed underneath the animal. The foot length, toe spread, and intermediary toe spread were measured for both the surgical and contralateral (control) sides. All three measurements were taken from the experimental and normal limbs, and the sciatic functional index (SFI)—commonly used to evaluate motor function recovery following sciatic nerve injury—was calculated as follows [24]:

$$\mathrm{SFI} = \frac{109.5(d_{\mathrm{ETS}} - d_{\mathrm{NTS}})}{d_{\mathrm{NTS}}} - \frac{38.3(d_{\mathrm{EPL}} - d_{\mathrm{NPL}})}{d_{\mathrm{NPL}}} + \frac{13.3(d_{\mathrm{EIT}} - d_{\mathrm{NIT}})}{d_{\mathrm{NIT}}} - 8.8.$$

Here, d represents the distance, "E" and "N" represent the experimental and normal sides, respectively. "TS" stands for toe spread, "PL" stands for foot length, and "IT" stands for intermediary toe spread.

2.12 Electrophysiological study

Before harvesting the repaired nerves, an electrophysiological study was conducted to evaluate the restored

nerve function following various treatments. The sciatic nerve on the operated side of the rats (under anesthesia) was adequately exposed. We recorded myoelectric activity using an electrophysiology system (BL-420, Yilian, Shanghai, China). Electrical stimulation (1 mA, 0.1 ms) was applied to the proximal end of the injured nerve to elicit action potentials in the gastrocnemius muscle (GM). The patterns of compound muscle action potentials (CMAPs) were then recorded and analyzed.

2.13 GM evaluation

Subsequently, the animals were euthanized, and the GMs from both sides were harvested. The wet weight of each muscle was measured, and its general appearance was photographed. The rate of muscle weight restoration was calculated as follows:

$$W_R = \frac{W_S}{W_N} \times 100\%.$$

Here, W_R is the rate of muscle weight restoration, and W_S and W_N represent the weight of the GM on the operated and normal (control) sides, respectively.

After weighing and photographing, the harvested GM tissues were divided into two halves. Each half was fixed in 4% PFA solution for 24 h, embedded in paraffin, sectioned (thickness: 6 μm), and subjected to Masson's trichrome staining. At least three sections were collected from each specimen for analysis. The percentage of collagen fiber area in the stained sections was calculated as follows:

$$c = \frac{b}{a+b} \times 100\%.$$

Here, a is the total cross-sectional area of the muscle fibers, b is the area of the collagen fibers, and c is the percentage of the collagen fiber area.

2.14 Transmission electron microscopy imaging

Transmission electron microscopy (TEM) imaging was conducted to examine the intricate structure of axons and myelin sheaths in the regenerated nerves within the conduits. A piece of rat sciatic nerve tissue (<1 mm^3) was fixed in a 4% glutaraldehyde solution and subsequently in a 1% osmium tetroxide solution. The samples were first dehydrated with ethanol at concentrations of 30%, 50%, 70%, 80%, 90%, and 95%, with each concentration applied for 15 min, followed by dehydration with anhydrous ethanol for 20 min. Next, the samples were incubated in acetone (SINOPHARM, China) for 20 min before being embedded in resin. The prepared samples were imaged using a transmission electron microscope (HT7700, Hitachi, Japan), and the thickness of the myelin sheath was measured using ImageJ.

2.15 Histological evaluation of regenerated nerve tissue

After acquiring samples for the TEM study, the remaining nerve tissues were fixed in a 4% PFA solution. The tissues were then dehydrated, embedded in paraffin, and sectioned into 5-μm slices. These sections underwent Sirius Red staining and immunohistochemical and immunofluorescent analyses. Briefly, antigen retrieval was conducted using a 0.01 mol/L citrate buffer (pH 6.0), followed by blocking with 5% goat serum at room temperature for 30 min. The sections were then incubated overnight at 4 °C with primary antibodies (anti-CD31, NF-H, S100β, and CD68) following the manufacturers' instructions. After washing with PBS, the sections were incubated with secondary antibodies in the dark at 37 °C for 1 h and then counterstained with DAPI to visualize the cell nuclei. The stained sections were examined using either a fluorescence microscope (for immunofluorescent imaging) or an optical microscope (for Sirius red staining and immunohistochemical analysis).

2.16 Western blotting

Cells grown on decellularized nerves were cultured to 80% confluence before being dissociated from the decellularized nerves matrix and lysed with a radio-immunoprecipitation assay (RIPA) lysis buffer. The resultant lysates were centrifuged for 15 min at 13,000 r/min, and the protein concentration in the supernatant was determined using a BCA kit (Thermo Scientific, 23225, USA). Approximately 15 μg of protein was separated through sodium dodecyl sulfate-polyacrylamide gel electrophoresis (SDS-PAGE) and transferred to polyvinylidene difluoride (PVDF) membranes. The membranes were blocked with 5% nonfat milk at room temperature for 1 h, followed by overnight incubation with primary antibodies—NF-H (1∶1000), GAP-43 (1∶1000), βIII-tubulin (1∶1000), PI3K (1∶1000), p-PI3K (1∶1000), Akt (1∶1000), p-Akt (1∶1000), and β-actin (1∶1000) diluted in 5% BSA solution. After rinsing with 0.05% Tris-borate-sodium Tween-20 (TBST) three times, the PVDF membranes were incubated with secondary antibodies for 1 h at room temperature. Finally, the membranes were treated with an enhanced chemiluminescence substrate (SQ201, EpiZyme Biotechnology, Shanghai, China), and the protein patterns were visualized using a chemiluminescence imaging system (Tanon 5200, Tanon, Taizhou, China).

2.17 Statistical analyses

Unless otherwise stated, all experiments were conducted in triplicate. Statistical analyses (Student's *t*-tests) were conducted using GraphPad Prism (Version 9.0.1, GraphPad Software, La Jolla, CA, USA), with results expressed as

mean±standard deviation. For the animal experiments, a one-way analysis of variance (ANOVA) was used to determine statistical significance. We considered $p<0.05$ statistically significant: $^{*}p<0.05$, $^{**}p<0.01$, $^{***}p<0.001$, and $^{****}p<0.0001$.

3 Results

3.1 Preparation and characterization of decellularized rat peripheral nerves

The process of decellularizing rat sciatic nerves is illustrated in Fig. 1a. To evaluate the effectiveness of this process, both native and decellularized nerve tissues were subjected to H&E staining. As shown in Fig. 1b, the decellularized tissues exhibited a highly porous structure, with nearly undetectable nuclei and cytoplasm of resident cells. SEM imaging revealed that the fibers in the dECM maintained considerable alignment (Fig. 1c, yellow arrows). Quantitative analysis indicated a substantial reduction in DNA content from 270 ng/mg to 4 ng/mg following decellularization, representing a decrease of (98.5±0.5)% (Fig. 1d). These results indicate that decellularization effectively removed cellular components from the sciatic nerves, yielding a dECM suitable for subsequent studies.

3.2 Viability and morphology of SCs seeded on dECM

To investigate the viability and morphology of SCs seeded on dECM in vitro, decellularized nerves were sliced into approximately 50-μm sections and adhered to PLL-coated coverslips, which served as a substrate for the SCs culture (Fig. 2a). SEM images (Fig. 2b) revealed that SCs were densely packed and well-adhered to the highly porous dECM after 3 d of culture. GFP signaling confirmed that the SCs were evenly distributed across the dECM (Fig. S1 in the supplementary information). Live/Dead staining was performed on Days 3 and 5 post-seeding to assess SC viability. As shown in Fig. 2c, the number of viable cells—stained with Calcein-AM (green)—increased over the culture period, while the number of dead cells—stained with PI (red)—remained minimal. Statistical analyses showed no significant difference in the percentage of dead cells between the dECM and control groups (Fig. 2d). Cell metabolic activity, assessed using the CCK-8 assay, indicated active proliferation of SCs seeded on the dECM (Fig. 2e). Collectively, these results demonstrate that dECM supports the adhesion, survival, and proliferation of seeded SCs.

3.3 Nerve conduit fabrication, mechanical testing, and in vivo application

Three experimental groups (PLGA, PLGA/dECM, and PLGA/dECM-SC) were established for nerve regeneration in a rat sciatic nerve defect model, with autologous nerve grafts as the control group. Figure 3a presents cross-sectional views of these NGCs and the surgical scheme. Their mechanical properties were evaluated through tensile testing. Figure 3b shows that the PLGA conduits exhibited a characteristic stress–strain curve, which included initial elastic deformation, followed by yielding, plastic deformation,

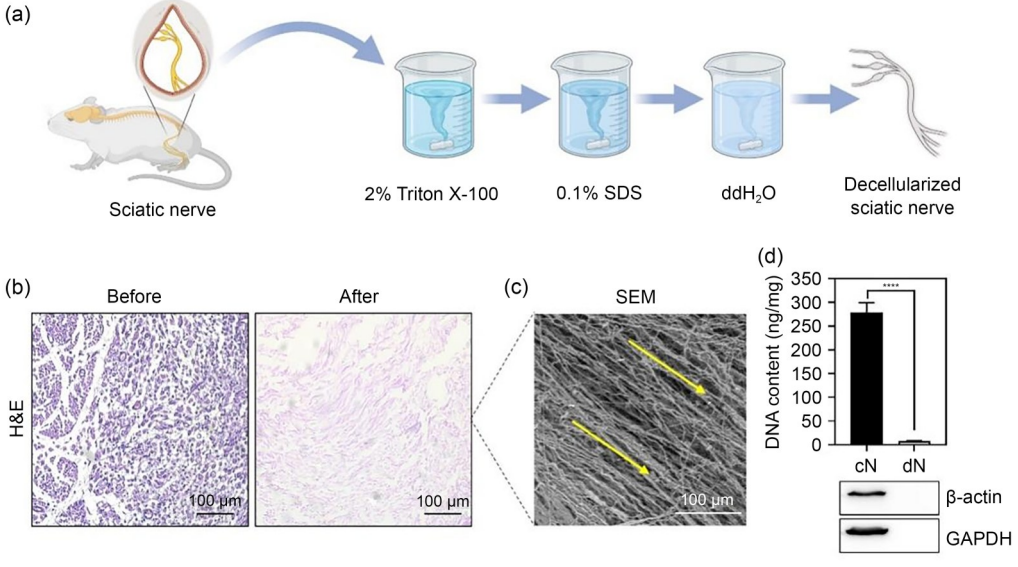

Fig. 1 Decellularization of rat nerves. (a) Schematic of the decellularization process. (b) H&E staining of rat sciatic nerves before and after decellularization. (c) Scanning electron microscope image of decellularized rat neural tissue. (d) Quantitative comparison of DNA content and Western blot analysis of housekeeping protein detection in neural tissue before and after decellularization (cN: control nerve; dN: decellularized nerve). Data are expressed as mean±standard deviation ($n=3$, $^{****}p<0.0001$)

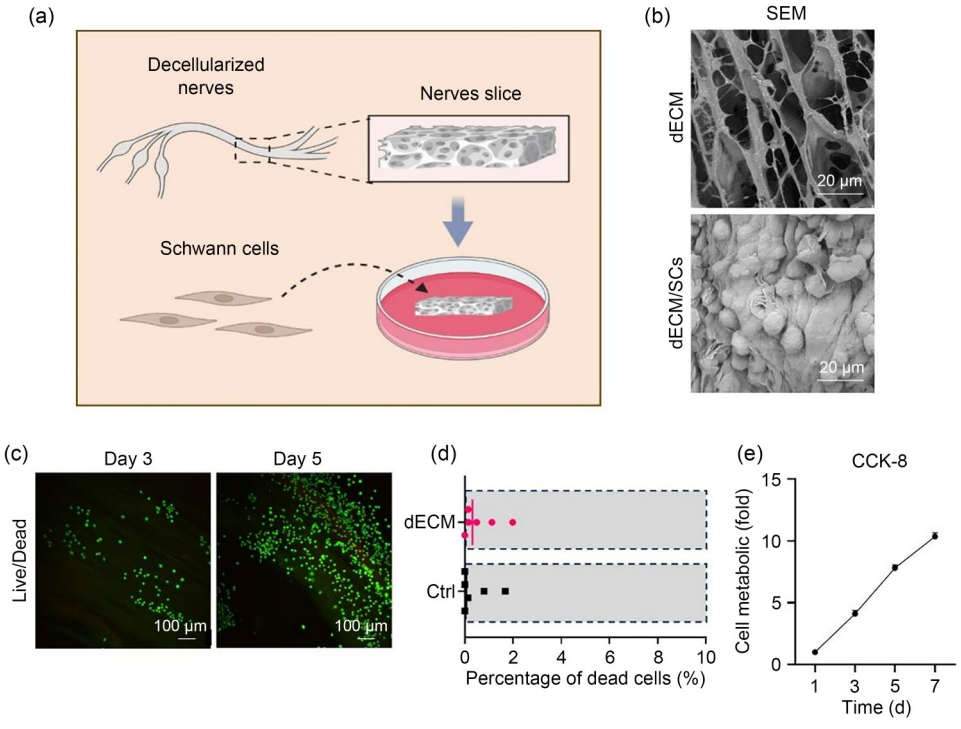

Fig. 2 In vitro culturing of SCs on dECM. (a) Schematic of preparing coverslips with dECM for in vitro cell culture. (b) SEM images of dECM and dECM seeded with SCs. (c) Live/Dead staining of SCs cultured on dECM. (d) Percentage of dead cells in the dECM and control groups (n=5). (e) Analysis of cell metabolic activity of SCs cultured on dECM

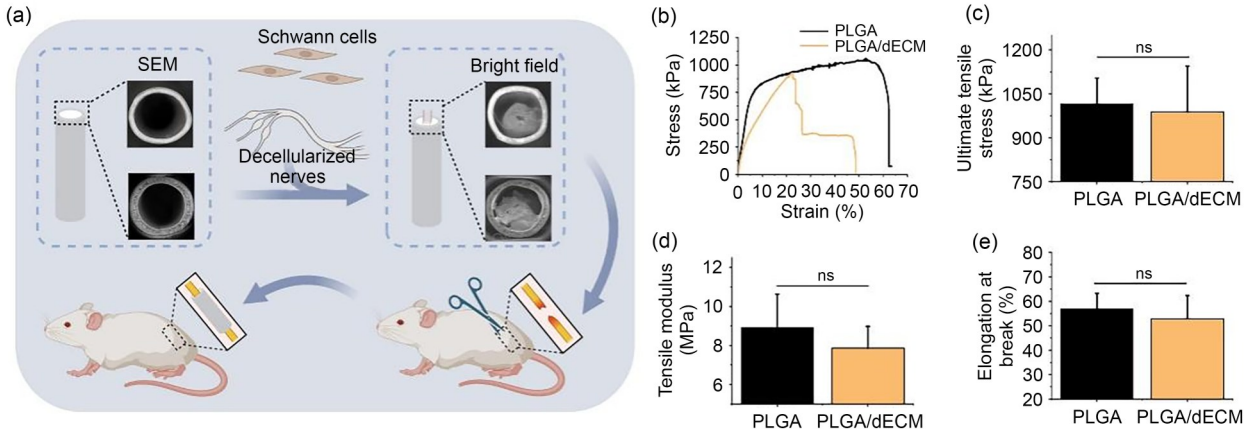

Fig. 3 Nerve regeneration in a rat sciatic nerve defect model and mechanical properties of PLGA and PLGA/dECM conduits. (a) Schematic of incorporating dECM into PLGA conduits and implanting the composite conduits in rats with PNI. (b) Representative stress–strain curves. (c) Ultimate tensile stress. (d) Nominal tensile modulus. (e) Elongation at break. Data are expressed as mean±standard deviation (n=3; ns: not significant)

and ultimately brittle fracture, indicated by a sudden decline in stress. Conversely, the PLGA/dECM conduits demonstrated a distinct stress profile characterized by multiple sharp declines in stress, likely due to the sequential rupture of the decellularized nerves and PLGA tubes. Figures 3c–3e show that incorporating the dECM resulted in marginal decreases in the ultimate tensile stress, tensile modulus, and elongation at break. However, these differences were not statistically significant among the experimental groups. In conclusion, dECM integration did not significantly affect the strength, stiffness, or flexibility of the conduits.

Following mechanical testing, the NGCs were transplanted into a rat sciatic nerve defect model to assess nerve regeneration. Figure S2a (supplementary information) shows photographs taken immediately after surgery, demonstrating suture-mediated anastomosis of nerve ends with grafts or NGCs. At 16 weeks post-surgery, the animals were euthanized, and their nerves were harvested for analysis.

Figure S2b (supplementary information) indicates that the nerve ends in all groups were well connected to either the grafts or NGCs. H&E staining of regenerated nerves was conducted, and cross-sectional areas were compared to assess the progress of nerve regeneration. The cross-sectional areas of the nerve fibers were similar between the autograft and PLGA/dECM-SC groups and were considerably larger than those in the other two groups, with the PLGA group showing the smallest cross-sectional area (Fig. S2c in the supplementary information). Sirius Red staining was also performed to evaluate collagen fiber content in the regenerated peripheral nerve. The PLGA/dECM-SC and PLGA/dECM groups exhibited collagen fiber levels comparable to those of the autograft group, while the PLGA group showed significantly lower collagen levels (Fig. S2d in the supplementary information).

Immunochemistry analysis of CD68 was conducted to evaluate macrophage infiltration in the regenerated peripheral nerves. Figure S3 (supplementary information) reveals a limited presence of CD68-positive cells in all groups, indicating a low inflammatory response following peripheral nerve recovery. Furthermore, GFP signals were imaged, showing detectable signals in the SC-transfected group, while few GFP signals were detected in the autograft group (Fig. S4 in the supplementary information). This suggests that transplanted SCs survived after 16 weeks. These results indicate that incorporating dECM promotes more effective peripheral nerve regeneration, which is further enhanced by seeding SCs. This combination resulted in nerve regeneration comparable to that achieved using autografts, highlighting its potential as a promising approach for PNI treatment.

3.4 Motor function analysis

Motor function was quantitatively assessed using the SFI. Footprints taken at 16 weeks post-surgery revealed that all animals exhibited reduced paw extension on the operated side compared to the non-operated side, indicating impaired motor function following PNI (Fig. 4a). Regarding postsurgical recovery, the highest SFI values were observed in the autograft group (−47.90), followed by the PLGA/dECM-SC (−53.84), PLGA/dECM (−62.87), and PLGA (−77.89) groups (Fig. 4d). The significantly higher SFI values in the PLGA/dECM-SC group compared to the other conduit-implanted groups indicate that both dECM and SCs facilitated the restoration of walking ability in rats with PNI.

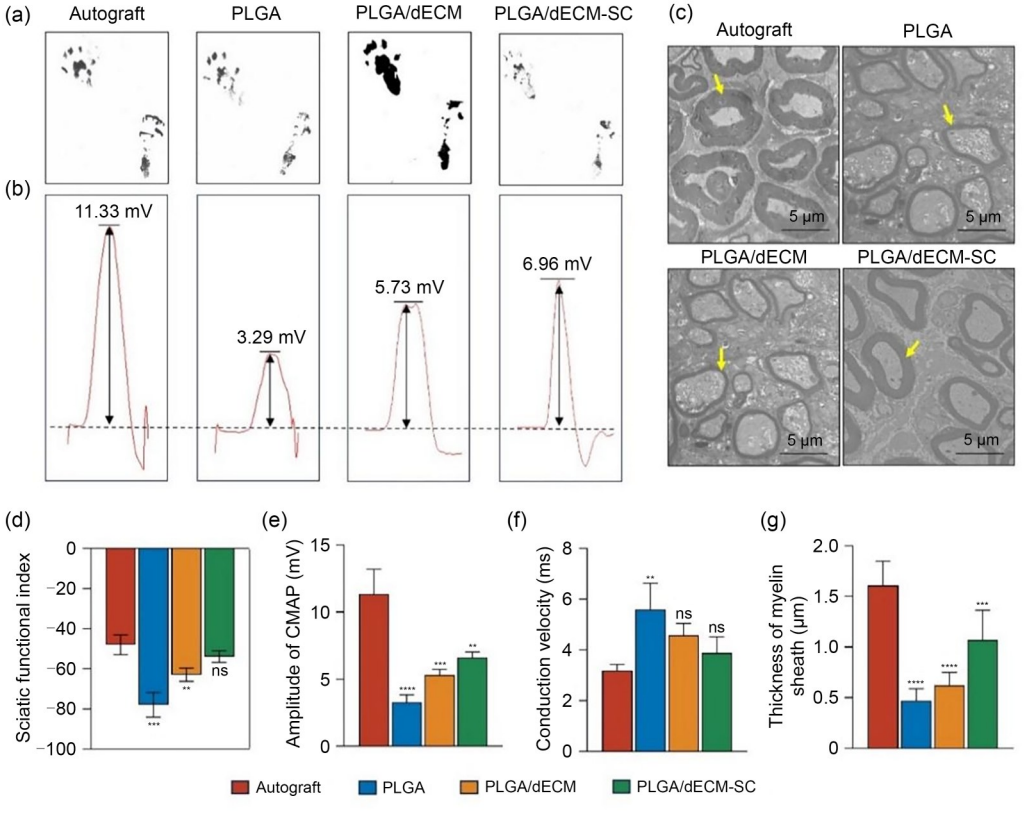

Fig. 4 Assessment of structural and functional recovery in the sciatic nerve at 16 weeks post-surgery. (a) Rat footprints showing unaffected (upper left) and treated (lower right) hind limbs. (b) Recorded CMAP patterns and amplitudes after surgical treatment. (c) TEM images of regenerated sciatic nerve axons. (d) SFI values for each treatment group (n=6). (e) CMAP amplitude values (n=6). (f) Latency time in response to electrical stimuli (n=6). (g) Thickness of myelin sheaths, as measured from TEM images (n=6). Data are expressed as mean±standard deviation. All significant p-values represent comparisons to the autograft group: $^{**}p<0.01$; $^{***}p<0.001$; $^{****}p<0.0001$. ns: not significant

Reinnervation of the regenerated nerves and restoration of nerve function were further assessed through electrophysiological studies. The highest CMAP amplitudes were observed in the autograft group (11.33 mV), followed by the PLGA/dECM-SC (6.96 mV), PLGA/dECM (5.73 mV), and PLGA (3.29 mV) groups (Figs. 4b and 4e). Additionally, the shortest latency time was found in the autograft group (3.2 ms), which was slightly shorter than that of the PLGA/dECM-SC group (3.9 ms; no statistical significance) and the PLGA/dECM group (4.6 ms; no statistical significance) but significantly shorter than that of the PLGA group (5.6 ms) (Fig. 4f).

TEM was used to visualize the ultrastructure of the regenerated sciatic nerve axons (Fig. 4c, yellow arrows), and the thickness of the myelin sheath was quantified (Fig. 4g). The myelin sheath thickness in the PLGA/dECM-SC group was the closest to that in the autograft group, while sheaths in the other two groups were noticeably thinner, corroborating the electrophysiological findings.

Collectively, these results indicate that combining dECM and SCs enhances nerve conduction capacity and motor function recovery. Although autografts provided the best treatment outcomes, the healing achieved using the PLGA-dECM/SC conduit was comparably effective, despite showing slightly lower efficacy.

3.5 GM analysis

To evaluate the impact of PNI and subsequent surgical treatments on GM reinnervation, GMs from both hind limbs were harvested at 16 weeks post-surgery. GMs on the operated side (right) were noticeably smaller than those on the unaffected side (left) across all groups, indicating substantial muscle atrophy following PNI (Fig. 5a). The extent of recovery, calculated as the weight ratio of the treated to the unaffected (control) GM, was highest in the autograft group (58.3%), followed by the PLGA-dECM/SC (42.6%), PLGA/dECM (38.8%), and PLGA (20.0%) groups (Fig. 5c).

Harvested GMs were then subjected to Masson's trichrome staining to examine muscle fiber (red) and collagen fiber (blue) distribution. Muscle fiber percentages were quantified using ImageJ. Compared to the autograft group, specimens from the PLGA group mostly contained collagen fibers, while GMs from the PLGA/dECM and PLGA/dECM-SC groups mostly contained muscle fibers (Figs. 5b and 5d). Notably, no significant differences were observed between the PLGA-dECM/SC and autograft groups, indicating that incorporating nerve ECM and SCs enhanced GM reinnervation, achieving results comparable to autograft treatment.

Overall, these findings demonstrate the efficacy of PLGA-dECM/SC conduits in promoting muscle recovery

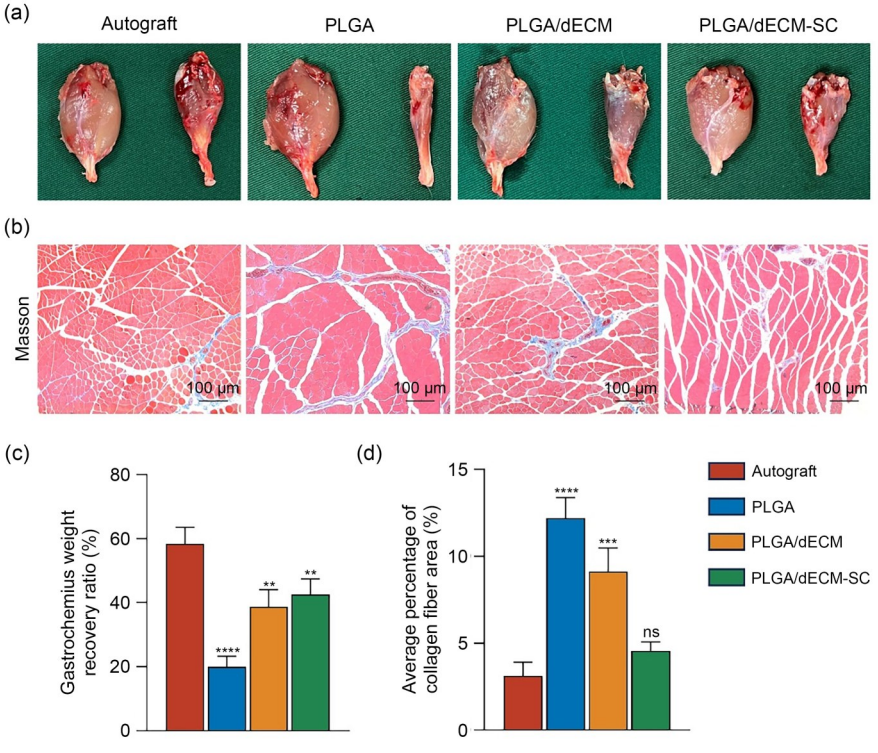

Fig. 5 Evaluation of GM reinnervation at 16 weeks post-surgery. (a) Images of GMs on the unaffected (left) and treated (right) sides of the hind limbs following different surgical treatments. (b) Masson's trichrome staining of GM on the treated side. (c) Recovery ratios of GMs based on GM weights (n=6). (d) Quantitative analysis of collagen fiber areas in stained GM sections (n=6). Data are expressed as mean±standard deviation. All significant p-values represent comparisons to the autograft group: $^{**}p<0.01$, $^{***}p<0.001$, $^{****}p<0.0001$. ns: not significant

and reinnervation following PNI, presenting a promising alternative to autografts in peripheral nerve repair.

3.6 Expression of proteins related to nerve regeneration in regenerated nerves

Western blotting was conducted to analyze the overall expression of proteins associated with nerve regeneration—NF-H, βIII-tubulin, and GAP-43—in the harvested tissues. Protein levels in the autograft and PLGA/dECM-SC groups were comparable, while the PLGA and PLGA/dECM groups exhibited considerably lower expression levels (Figs. 6a–6d). Immunofluorescence staining was utilized to visualize the expression of S100β and NF-H, specific biomarkers for myelin glial cells and neurofilaments, respectively. Positive staining for both S100β and NF-H was evenly distributed across regenerated nerves in all groups (Fig. 6e). Notably, the autograft and PLGA/dECM-SC groups displayed similar levels of staining intensity, contrasting with the significantly lower intensity in the other two groups. These findings were confirmed by quantitative analysis of the immunofluorescence staining intensity, performed using ImageJ and normalized to the area (Figs. 6f and 6g).

To assess the blood vessel formation accompanying nerve regeneration, we analyzed the expression of CD31, a key biomarker for blood vessels. Figures S5a and S5b (supplementary information) show that the autograft and PLGA/dECM-SC groups exhibited significantly higher CD31-positive areas than the PLGA and PLGA/dECM groups. Additionally, the angiogenic potential of SCs cultured on dECM was assessed through HUVEC migration and tube formation assays in vitro. HUVECs were placed in Transwell chambers with different conditioned media in the lower chambers, and cell migration was determined by staining. Media from dECM-cultured SCs exhibited significantly stronger chemotaxic effects on HUVECs compared with the control at 12 h (Fig. S6a in the supplementary information), with quantification confirming this difference (Fig. S6b in the supplementary information). A tube formation assay further evaluated the impact of conditioned media from dECM-cultured SCs on HUVEC angiogenesis. HUVECs treated with this medium demonstrated significantly enhanced tube formation compared with the control group, with quantification of branch points yielding similar results (Figs. S6c and S6d in the supplementary information). Overall, these data indicate that the inclusion of dECM and SCs in NGCs improves angiogenesis, axonal regeneration, and cell differentiation, providing a promising alternative for peripheral nerve repair with regenerative potential closely resembling that of autografts.

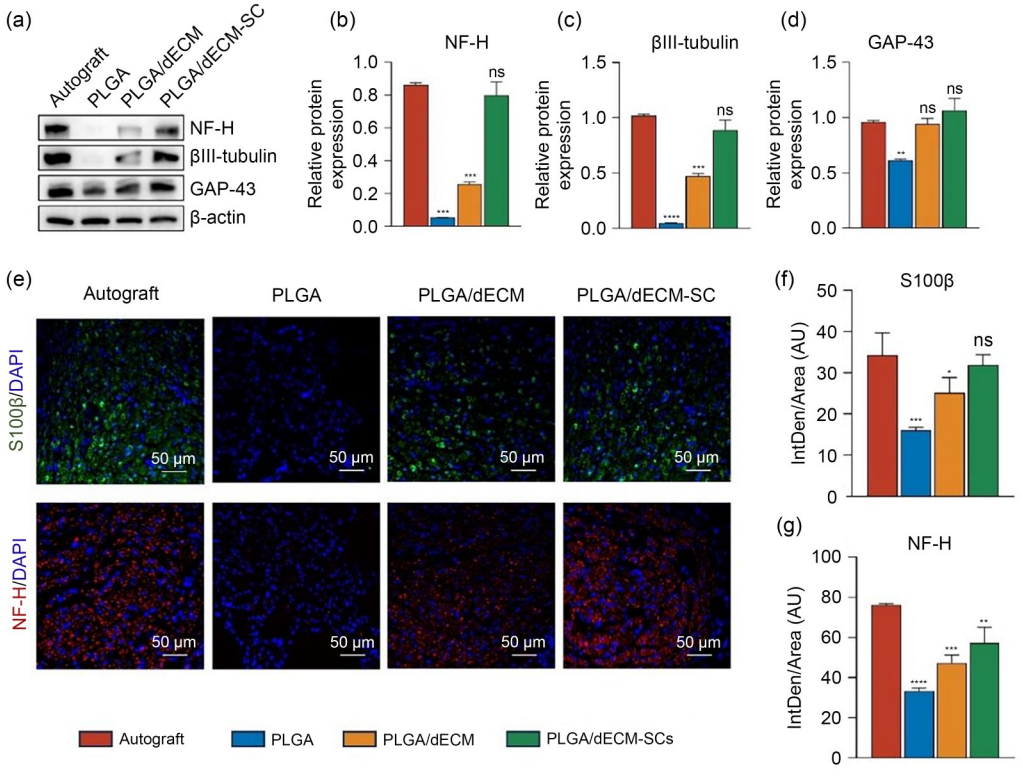

Fig. 6 Expression of proteins related to nerve regeneration post-surgery. (a–d) Western blot images and quantifications of NF-H, βIII-tubulin, and GAP-43 (n=3). (e) Immunofluorescence staining for S100β and NF-H in nerves following surgical treatments. Quantitative analysis of immunofluorescence staining for S100β (f) and NF-H (g) (n=6). Data are expressed as mean±standard deviation. All significant p-values represent comparisons to the autograft group: $^{*}p<0.05$, $^{**}p<0.01$, $^{***}p<0.001$, $^{****}p<0.0001$. ns: not significant

3.7 Function of dECM on SCs

In vitro studies were conducted to investigate the effects of dECM on SC morphology, proliferation, and functions relevant to nerve regeneration. As shown in Fig. S7a (supplementary information), SCs became more densely packed as the culturing period was extended, with cytoskeletons, stained by phalloidin (green) exhibiting elongated morphologies. This observation suggests that the dECM, characterized by an aligned fibrous structure, supports SC proliferation and alignment. Similar alignment effects were observed in DRGs, which demonstrated notable axon extension when cultured on the dECM substrate (Fig. 7a). Regarding their proliferative activity, SCs cultured on dECM showed elevated mRNA levels of *Ki67* expression, although this increase was not statistically significant (Fig. 7b). Regarding their role in nerve regeneration, SCs cultured on dECM expressed higher levels of *NF-H* and *GAP-43* than those cultured on blank coverslips (control). Similarly, protein levels of NF-H, GAP-43, and βIII-tubulin were upregulated in SCs cultured on dECM (Fig. 7c), with quantification data provided in Fig. S7b (supplementary information). Furthermore, the secretion of neurotrophic factors NGF, BDNF, and GDNF, analyzed by ELISA kits, was higher in the dECM-cultured SCs (Fig. 7d). We also analyzed the PI3K/Akt signaling pathway, which regulates cellular functions, including growth, survival, metabolism, and proliferation. Western blot data (Fig. 7e) demonstrated PI3K/Akt activation in SCs cultured on dECM, with quantification data shown in Figs. 7f and 7g.

In summary, these results indicate that dECM promotes SC function by supporting its proliferation, inducing cytoskeletal elongation, and upregulating nerve-regenerative genes. These biological activities are considered essential for PNI healing. Hence, dECM shows promise as a substrate for enhancing SC function in nerve repair, potentially through the activation of the PI3K/Akt signaling pathway.

4 Discussion

PNIs with significant gaps between nerve ends present a significant clinical challenge, necessitating novel treatments that match the effectiveness of neural autografts without the

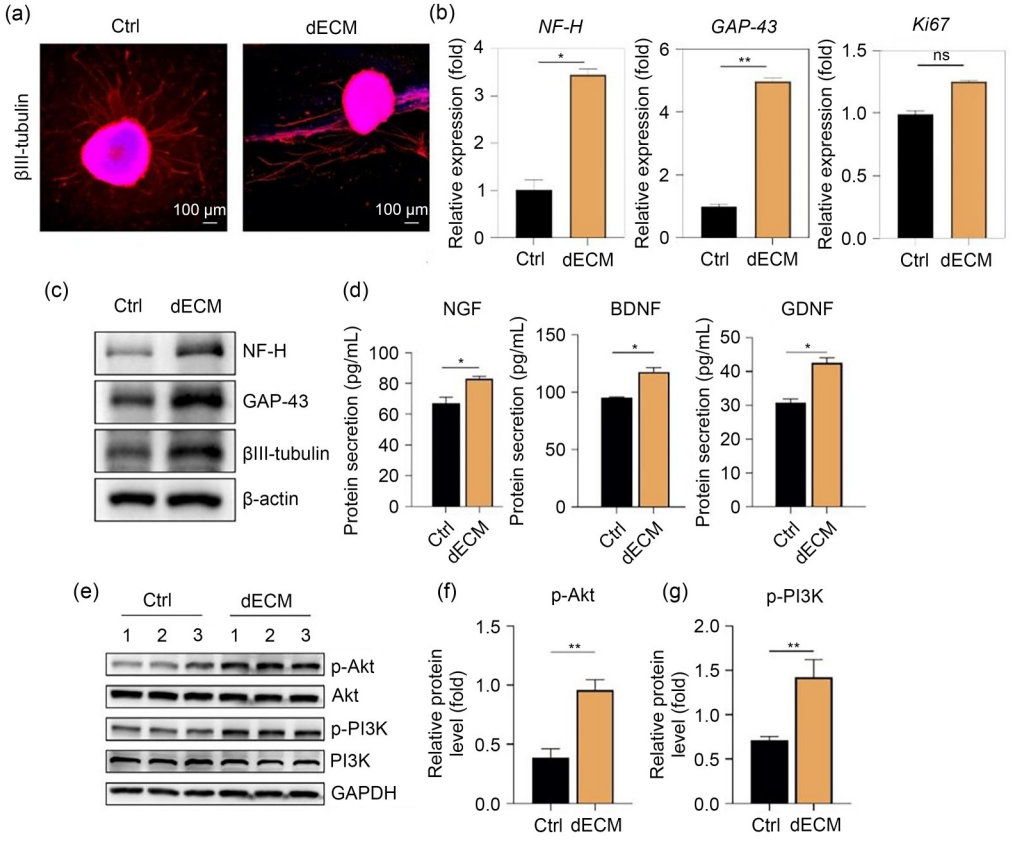

Fig. 7 Effects of dECM on SC morphology and gene expression. (a) Axon extension testing using DRGs cultured on dECM and blank plates. (b) qPCR analysis showing mRNA expression levels of *NF-H*, *GAP-43*, and *Ki67* in SCs cultured on dECM compared with the control (n=3). (c) Western blot analysis of NF-H, GAP-43, and βIII-tubulin protein levels in SCs. (d) ELISA-based detection of neurotrophic factor secretion (n=3). (e) Western blot analysis of p-Akt (Akt) and p-PI3K (PI3K) protein levels in SCs. Quantitative analysis of p-Akt (f) and p-PI3K (g) expression (n=3). Data are expressed as mean±standard deviation; $^{*}p<0.05$, $^{**}p<0.01$. ns: not significant; qPCR: quantitative polymerase chain reaction

issues of limited availability and donor site morbidity. Although synthetic polymer nerve conduits can physically guide the reconnection of injured nerves, their efficacy is often limited by insufficient bioactivity, which is essential for enhancing regeneration. This highlights the need for additional biological [25, 26] or chemical [27] cues to stimulate the repair process. To address this, we integrated dECM loaded with SCs from sciatic nerves into PLGA-based nerve conduits to enhance bioactivity. This study demonstrated that the composite conduits significantly outperformed bare PLGA conduits in promoting peripheral nerve regeneration, as evidenced by the restoration of structural integrity and neurological function.

The value of ECM in regenerative medicine is well recognized due to its excellent biomimetic properties and rich biochemical composition, which facilitate tissue regeneration [28, 29]. For instance, Guan et al. found that modifying PCL/silk fibroin electrospun nanofibers with ECM derived from human umbilical cord mesenchymal stem cells led to highly effective peripheral nerve repair, largely due to the bioactive molecules preserved in the ECM [30]. Additionally, dECM has been reported to significantly lower the ratio of proinflammatory M1 macrophages to proregenerative M2 macrophages, thereby facilitating the healing of spinal cord injury [31]. Similarly, Tian et al. reported that dECM promotes axon regeneration and remyelination in the recovery of transected spinal cords [32]. Our previous research supports this approach, showing that decellularized rat nerves promote the unidirectional extension and proliferation of PC-12 cells [33] and effectively enhance the healing of sciatic nerve injuries in rats when incorporated into PLGA conduits [8].

The decellularized sciatic nerves in this study exhibited a highly porous structure, with fibers generally aligned in a single direction (Figs. 1c, 2b, and 7a). This structural characteristic is believed to enhance neuronal adhesion and growth while physically guiding axon extension [34]. The importance of physical guidance cues in healing nerve defects was well documented in the literature [35–37]. Moreover, studies have shown that the decellularization process removes proteins that inhibit axon growth while preserving those that facilitate neurite growth, thereby enhancing nerve regeneration [38]. However, ensuring the complete removal of cells and DNA from the original tissues is crucial, as residual components can be highly immunogenic and increase the risk of graft rejection after implantation [39]. In this study, the decellularization process successfully reduced residual DNA by 98.5%, and similar results were observed in GAPDH and β-actin protein levels (Fig. 1d), resulting in dECM with low immunogenicity suitable for subsequent implantation.

In the in vivo study, the PLGA/dECM-SC conduits outperformed both the PLGA and PLGA/dECM groups in promoting effective nerve regeneration. This superiority was confirmed through histological staining, motor function analysis, and nerve conduction tests. Histological analysis of axon elongation and myelination provides valuable insights into the progress of nerve regeneration [40]. The elongation of axons to reach target cells or tissues is pivotal in re-establishing functional neural connections [41], whereas myelination, characterized by the formation of a thick myelin sheath, is crucial for rapid nerve signal transmission [42]. Histological findings revealed increased axonal growth, well-organized nerve fibers, and thicker myelin sheaths following treatment with the PLGA/dECM-SC conduits. These findings suggest that the dECM and SCs create an environment conducive to peripheral nerve regeneration. Correspondingly, rats treated with the PLGA/dECM-SC conduits demonstrated higher nerve conduction velocities and improved restoration of motor function.

In addition to histological analysis, the in vivo expression of nerve growth-related genes—*NF-H*, *S100β*, *GAP-43*, and *βIII-tubulin*—was investigated. *NF-H*, a major component of the neuronal cytoskeleton, provides structural support to axons and regulates axon diameter [43]. *GAP-43* is actively expressed during nerve regeneration to enhance axonal growth and synaptic plasticity [43]. The quantitative polymerase chain reaction (qPCR) results indicated that the expression of these genes in SCs was upregulated when cultured on dECM (Fig. 7b). A more pronounced expression was also observed in the Western blot images (Fig. 7c). Additionally, neurotrophic factor secretion was higher in the dECM-cultured SC group than in the control group (Fig. 7d), suggesting increased proliferative activity of SCs in the tissue samples. βIII-tubulin, a molecule synthesized in the first two weeks following nerve injury to support axonal regrowth, also showed upregulated expression in the presence of dECM [44]. These findings demonstrate that dECM stimulates SC activities related to nerve regeneration, ultimately leading to the restoration of neurological function in vivo.

Additionally, the activation of the PI3K/Akt signaling pathway was investigated to explore the molecular mechanisms underlying the positive effects of dECM on SCs. The Western blot results demonstrated significant upregulation of key components of the PI3K/Akt pathway in dECM-cultured SCs (Figs. 7e–7g), suggesting that dECM enhances SC proliferation, survival, and neurotrophic factor secretion through this pathway. Given that the PI3K/Akt pathway is crucial for regulating cellular processes such as growth, survival, and metabolism, its activation likely contributes significantly to the improved nerve regeneration observed in our study. These findings provide insight into the molecular basis of how dECM supports SC behavior, reinforcing the potential of dECM-based conduits to enhance peripheral nerve

repair through a bioactive and mechanistically driven approach. Moreover, CD31 expression was more pronounced following repair with autografts and PLGA/dECM-SC composite NGCs, as shown in the immunohistochemical analysis (Fig. 6e). CD31, also known as platelet endothelial cell adhesion molecule-1, plays a key role in forming new blood vessels and maintaining vascular integrity. CD31-mediated angiogenesis likely contributed to vascularization, which is crucial for transporting nutrients and oxygen necessary for nerve regeneration [45]. This finding is supported by similar data showing the migration and tube formation of HUVECs (Figs. S6a–S6d in the supplementary information).

Notably, preventing regenerating nerves from mechanical irritation and invading fibrous tissue is crucial for supporting axonal growth. To ensure the biocompatibility, biodegradability, and adequate mechanical strength of the NGCs, we employed PLGA—a synthetic biopolymer approved by the United States Food and Drug Administration (FDA) for clinical applications as a drug carrier—for conduit fabrication [46]. In this study, the PLGA conduit sutured to the injured nerves not only enclosed the nerve ends but also prevented surrounding fibrous tissue from invading, which could impede the reconnection of injured nerves. Microscopic images showed that the dECM adhered well to the PLGA conduits, with no visible gaps.

Although the efficacy of these composite NGCs has only been validated in animal models, they show significant potential for clinical translation. The dry jet-wet spinning process has proven to be a robust and economical method for upscaling PLGA conduit production [47]. In addition, there is increasing interest in the clinical application of decellularized cadaver-derived human nerve allografts [48, 49], which offer efficacy comparable to autologous nerve grafts while reducing donor site morbidity and costs [50, 51]. Despite these advantages, PLGA/dECM conduits cannot sustainably provide bioactive cues (e.g., cytokines, extracellular proteins, and exosomes [52]) to the injury site. This limitation hinders their ability to support long-term axonal growth and myelination [53, 54]. To address this, viable SCs were incorporated into the composite NGCs. We hypothesized that SCs, which could potentially be harvested in the future from human adipose stem cells and human-induced pluripotent stem cells (hiPSCs) less invasively [55, 56], can remodel the ECM and release additional growth factors and cytokines, thereby synergizing with dECM to enhance tissue regeneration.

Our proposed composite NGC offers several potential advantages over clinically approved NGCs. A key feature is the incorporation of nerve-derived ECM, which significantly enhances the colonization and subsequent regenerative activities of SCs, whether they are seeded or locally recruited. The PLGA component of the conduit also contributes significantly to repairing nerve defects. Compared to polyglycolic acid, the primary component of NeuroTube®, the copolymerization with polylactic acid results in decreased crystallinity and increased hydrophobicity in PLGA [57]. This process reduces the degradation rate of the NGC, mitigating the risk of acute pH reduction, which can cause pain and impede healing [58]. In vivo studies have also demonstrated that PLGA conduits exhibit comparable efficacy and safety profiles to the FDA-approved Neurolac® conduits in facilitating regeneration following sciatic nerve injury in rats [59]. While collagen, another naturally derived material, offers excellent biocompatibility and low immunogenicity, it has limited mechanical strength and degrades rapidly [60]. In contrast, our PLGA-based NGC, with its superior strength and stiffness, offers greater stability and prevents nerve compression due to conduit collapse [61, 62]. However, a long-term follow-up study is necessary to elucidate the extended safety profile of the studied composite NGC.

Despite the promising results, several limitations of our study must be addressed. First, while the rat sciatic nerve model provides valuable insights, its clinical relevance has limitations. Rat models, especially those with 6–10 mm nerve gaps, are widely used due to their low cost and ease of handling [63]. However, the regenerative capacity of rodents far exceeds that of humans, and these models do not accurately replicate the critical nerve gaps observed in clinical cases [64]. Therefore, the efficacy of the PLGA/dECM-SC conduit should be further validated in larger animal models, such as dogs, sheep, and pigs—which more closely resemble human nerve injuries. These studies should also involve longer observation periods to assess nerve regeneration over larger gaps and ensure clinical applicability before progressing to human trials. Second, the small sample size of the animal model may limit the statistical power and generalizability of our findings. Increasing the number of animals in future studies will facilitate more robust conclusions. Third, the long-term biocompatibility and degradation profile of the PLGA/dECM-SC conduit were not fully elucidated within the 16-week study period. Future studies should focus on assessing the safety, immune response, and efficacy of the conduit over extended periods. Furthermore, preventing SC senescence during cell harvesting is crucial [65, 66], as aging SCs exhibit diminished regenerative capacity. Finally, future research should explore the integration of advanced bioengineering strategies to further enhance nerve regeneration. This includes the controlled release of neurotrophic factors and the incorporation of genetically modified SCs that overexpress genes beneficial for nerve repair. These enhancements could significantly improve the regenerative potential of NGCs and lead to improved clinical outcomes.

5 Conclusions

In this study, we developed PLGA-based composite NGCs incorporating dECM from rat sciatic nerves and viable SCs to treat PNIs in rats. The PLGA component provided structural support, while the dECM served as a bioactive substrate that promoted SC adhesion, elongation, and proliferation. The dECM also upregulated genes associated with nerve regeneration. Incorporating SCs into the NGCs further enhanced the regeneration of the structural and functional features of peripheral nerves, leading to improved myelination, restored motor function, enhanced nerve conduction, and increased local vascularization compared to acellular conduits. The activation of the PI3K/Akt signaling pathway likely underlies these regenerative effects. Our findings highlight the crucial role of the nerve ECM and viable SCs in promoting nerve regeneration and offer a promising approach for clinical applications in PNI treatment.

Supplementary Information The online version contains supplementary material available at https://doi.org/10.1631/bdm.2400334.

Acknowledgements The authors gratefully acknowledge the support provided by the Ningbo Natural Science Foundation (No. 2023J137), the Natural Science Foundation of Zhejiang Province (No. BY23H180015), and the Zhejiang Medical Science and Technology Project (Nos. 2022KY1101 and 2022KY111).

Author contributions ZFX: data curation, formal analysis, writing—original draft, and writing—review & editing. YYH: conceptualization, data curation, formal analysis, writing—original draft, writing—review & editing, and funding acquisition. DB: data curation and formal analysis. KY: data curation and writing—original draft. HYZ and LZH: data curation and software. PW: funding acquisition, resources, supervision, writing—review & editing, and conceptualization. YJW: conceptualization, funding acquisition, project administration, supervision, and writing—review & editing.

Declarations

Conflict of interest The authors declare that they have no conflict of interest.

Ethical approval All experimental procedures were approved by the Institutional Animal Care and Use Committee (IACUC) of Ningbo University (NBU, No. 12213).

Data availability The data that support the findings of this study are available from the corresponding authors upon reasonable request.

References

1. Henderson WR (1948) Clinical assessment of peripheral nerve injuries Tinel's test. Lancet 252(6534):801–805. https://doi.org/10.1016/S0140-6736(48)91379-8
2. Liu B, Xin W, Tan JR et al (2019) Myelin sheath structure and regeneration in peripheral nerve injury repair. Proc Natl Acad Sci USA 116(44):22347–22352. https://doi.org/10.1073/pnas.1910292116
3. Dai Y, Lu TW, Li LL et al (2024) Electrospun composite PLLA-PPSB nanofiber nerve conduits for peripheral nerve defects repair and regeneration. Adv Healthc Mater 13(10):e2303539. https://doi.org/10.1002/adhm.202303539
4. Kornfeld T, Nessler J, Helmer C et al (2021) Spider silk nerve graft promotes axonal regeneration on long distance nerve defect in a sheep model. Biomaterials 271:120692. https://doi.org/10.1016/j.biomaterials.2021.120692
5. Quan Q, Meng HY, Chang B et al (2019) Aligned fibers enhance nerve guide conduits when bridging peripheral nerve defects focused on early repair stage. Neur Regen Res 14(5):903–912. https://doi.org/10.4103/1673-5374.249239
6. Vijayavenkataraman S, Thaharah S, Zhang S et al (2019) Electrohydrodynamic jet 3D-printed PCL/PAA conductive scaffolds with tunable biodegradability as nerve guide conduits (NGCs) for peripheral nerve injury repair. Mater Des 162:171–184. https://doi.org/10.4103/1673-5374.249239
7. Han Y, Yin J (2022) Industry news: the additive manufacturing of nerve conduits for the treatment of peripheral nerve injury. Bio-Des Manuf 5(1):6–8. https://doi.org/10.1007/s42242-021-00166-z
8. Yu EX, Chen ZW, Huang YY et al (2023) A grooved conduit combined with decellularized tissues for peripheral nerve regeneration. J Mater Sci Mater Med 34(7):35. https://doi.org/10.1007/s10856-023-06737-z
9. Fang YC, Wang CJ, Liu ZB et al (2023) 3D printed conductive multiscale nerve guidance conduit with hierarchical fibers for peripheral nerve regeneration. Adv Sci 10(12):e2205744. https://doi.org/10.1002/advs.202205744
10. Carvalho CR, Costa JB, Costa L et al (2019) Enhanced performance of chitosan/keratin membranes with potential application in peripheral nerve repair. Biomater Sci 7(12):5451–5466. https://doi.org/10.1039/C9BM01098J
11. Zhang SJ, Wang J, Zheng ZZ et al (2021) Porous nerve guidance conduits reinforced with braided composite structures of silk/magnesium filaments for peripheral nerve repair. Acta Biomater 134:116–130. https://doi.org/10.1016/j.actbio.2021.07.028
12. Li X, He N, Li XJ et al (2023) Graphdiyne-loaded polycaprolactone nanofiber scaffold for peripheral nerve regeneration. J Colloid Interface Sci 646:399–412. https://doi.org/10.1016/j.jcis.2023.05.054
13. Mei Q, Yuen HY, Zhao X (2022) Mechanical stretching of 3D hydrogels for neural stem cell differentiation. Bio-Des Manuf 5(4):714–728. https://doi.org/10.1007/s42242-022-00209-z
14. Li T, Javed R, Ao Q (2021) Xenogeneic decellularized extracellular matrix-based biomaterials for peripheral nerve repair and regeneration. Curr Neuropharmacol 19(12):2152–2163. https://doi.org/10.2174/1570159X18666201111103815
15. Wang SS, Wang HK, Lu PJ et al (2024) Mechanisms underlying the cell-matrixed nerve grafts repairing peripheral nerve defects. Bioact Mater 31:563–577. https://doi.org/10.1016/j.bioactmat.2023.09.002
16. Golebiowska AA, Intravaia JT, Sathe VM et al (2024) Decellularized extracellular matrix biomaterials for regenerative therapies: advances, challenges and clinical prospects. Bioact Mater 32:98–123. https://doi.org/10.1016/j.bioactmat.2023.09.017
17. Yan LZ, Liu S, Wang JW et al (2024) Constructing nerve guidance conduit using dECM-doped conductive hydrogel to promote peripheral nerve regeneration. Adv Funct Mater 34(38): 2402698. https://doi.org/10.1002/adfm.202402698
18. Binan L, Tendey C, de Crescenzo G et al (2014) Differentiation

of neuronal stem cells into motor neurons using electrospun poly-L-lactic acid/gelatin scaffold. Biomaterials 35(2):664–674. https://doi.org/10.1016/j.biomaterials.2013.09.097
19. Li Y, Men YZ, Wang BX et al (2020) Co-transplantation of Schwann cells and neural stem cells in the laminin-chitosan-PLGA nerve conduit to repair the injured recurrent laryngeal nerve in SD rats. J Mater Sci Mater Med 31(11):99. https://doi.org/10.1007/s10856-020-06436-z
20. Aszmann OC, Korak KJ, Luegmair M et al (2008) Bridging critical nerve defects through an acellular homograft seeded with autologous Schwann cells obtained from a regeneration neuroma of the proximal stump. J Reconstr Microsurg 24(3):151–158. https://doi.org/10.1055/s-2008-1076091
21. Gonzalez-Perez F, Hernández J, Heimann C et al (2018) Schwann cells and mesenchymal stem cells in laminin- or fibronectin-aligned matrices and regeneration across a critical size defect of 15 mm in the rat sciatic nerve. J Neurosurg Spine 28(1):109–118. https://doi.org/10.3171/2017.5.SPINE161100
22. Cerqueira SR, Lee YS, Cornelison RC et al (2018) Decellularized peripheral nerve supports Schwann cell transplants and axon growth following spinal cord injury. Biomaterials 177:176–185. https://doi.org/10.1016/j.biomaterials.2018.05.049
23. Funk D, Fricke C, Schlosshauer B (2007) Aging Schwann cells in vitro. Eur J Cell Biol 86(4):207–219. https://doi.org/10.1016/j.ejcb.2006.12.006
24. Huang YY, Ye K, He AD et al (2024) Dual-layer conduit containing VEGF-A-transfected Schwann cells promotes peripheral nerve regeneration via angiogenesis. Acta Biomater 180:323–336. https://doi.org/10.1016/j.actbio.2024.03.029
25. Lackington WA, Kočí Z, Alekseeva T et al (2019) Controlling the dose-dependent, synergistic and temporal effects of NGF and GDNF by encapsulation in PLGA microparticles for use in nerve guidance conduits for the repair of large peripheral nerve defects. J Contr Release 304:51–64. https://doi.org/10.1016/j.jconrel.2019.05.001
26. Labroo P, Shea J, Edwards K et al (2017) Novel drug delivering conduit for peripheral nerve regeneration. J Neur Eng 14(6): 066011. https://doi.org/10.1088/1741-2552/aa867d
27. Xu TM, Chu HY, Li M et al (2022) Establishment of FK506-enriched PLGA nanomaterial neural conduit produced by electrospinning for the repair of long-distance peripheral nerve injury. J Nanomater 2022(1):3530620. https://doi.org/10.1155/2022/3530620
28. Yu TH, Ao Q, Ao TR et al (2023) Preparation and assessment of an optimized multichannel acellular nerve allograft for peripheral nerve regeneration. Bioeng Transl Med 8(4):e10435. https://doi.org/10.1002/btm2.10435
29. Wang SR, Zhu CL, Zhang B et al (2022) BMSC-derived extracellular matrix better optimizes the microenvironment to support nerve regeneration. Biomaterials 280:121251. https://doi.org/10.1016/j.biomaterials.2021.121251
30. Guan YJ, Ren ZQ, Yang BY et al (2023) Dual-bionic regenerative microenvironment for peripheral nerve repair. Bioact Mater 26:370–386. https://doi.org/10.1016/j.bioactmat.2023.02.002
31. Cornelison RC, Gonzalez-Rothi EJ, Porvasnik SL et al (2018) Injectable hydrogels of optimized acellular nerve for injection in the injured spinal cord. Biomed Mater 13(3):034110. https://doi.org/10.1088/1748-605X/aaab82
32. Tian T, Yu ZH, Zhang NL et al (2017) Modified acellular nerve-delivering PMSCs improve functional recovery in rats after complete spinal cord transection. Biomater Sci 5(12):2480–2492. https://doi.org/10.1039/c7bm00485k
33. Ye K, He AD, Wu MB et al (2022) In vitro study of decellularized rat tissues for nerve regeneration. Front Neurol 13:986377. https://doi.org/10.3389/fneur.2022.986377
34. Kim IG, Hwang MP, Park JS et al (2019) Stretchable ECM patch enhances stem cell delivery for post-MI cardiovascular repair. Adv Healthc Mater 8(17):e1900593. https://doi.org/10.1002/adhm.201900593
35. Ma YZ, Zhang RZ, Mao XY et al (2024) Preparation of PLCL/ECM nerve conduits by electrostatic spinning technique and evaluation in vitro and in vivo. J Neur Eng 21(2):026028. https://doi.org/10.1088/1741-2552/ad3851
36. Huang LL, Gao JB, Wang HR et al (2020) Fabrication of 3D scaffolds displaying biochemical gradients along longitudinally oriented microchannels for neural tissue engineering. ACS Appl Mater Interfaces 12(43):48380–48394. https://doi.org/10.1021/acsami.0c15185
37. Ning LQ, Sun HY, Lelong T et al (2018) 3D bioprinting of scaffolds with living Schwann cells for potential nerve tissue engineering applications. Biofabrication 10(3):035014. https://doi.org/10.1088/1758-5090/aacd30
38. Sun JH, Li G, Wu TT et al (2020) Decellularization optimizes the inhibitory microenvironment of the optic nerve to support neurite growth. Biomaterials 258:120289. https://doi.org/10.1016/j.biomaterials.2020.120289
39. Keane TJ, Londono R, Turner NJ et al (2012) Consequences of ineffective decellularization of biologic scaffolds on the host response. Biomaterials 33(6):1771–1781. https://doi.org/10.1016/j.biomaterials.2011.10.054
40. Nave KA (2010) Myelination and support of axonal integrity by glia. Nature 468(7321):244–252. https://doi.org/10.1038/nature09614
41. Mar FM, Bonni A, Sousa MM (2014) Cell intrinsic control of axon regeneration. EMBO Rep 15(3):254–263. https://doi.org/10.1002/embr.201337723
42. Chang W, Shah MB, Lee P et al (2018) Tissue-engineered spiral nerve guidance conduit for peripheral nerve regeneration. Acta Biomater 73:302–311. https://doi.org/10.1016/j.actbio.2018.04.046
43. Albayar AA, Roche A, Swiatkowski P et al (2019) Biomarkers in spinal cord injury: prognostic insights and future potentials. Front Neurol 10:27. https://doi.org/10.3389/fneur.2019.00027
44. Moskowitz PF, Oblinger MM (1995) Sensory neurons selectively upregulate synthesis and transport of the beta III-tubulin protein during axonal regeneration. J Neurosci 15(2):1545–1555. https://doi.org/10.1523/jneurosci.15-02-01545.1995
45. Qian Y, Gong JX, Lu KJ et al (2023) DLP printed hDPSC-loaded GelMA microsphere regenerates dental pulp and repairs spinal cord. Biomaterials 299:122137. https://doi.org/10.1016/j.biomaterials.2023.122137
46. Makadia HK, Siegel SJ (2011) Poly lactic-co-glycolic acid (PLGA) as biodegradable controlled drug delivery carrier. Polymers 3(3):1377–1397. https://doi.org/10.3390/polym3031377
47. Yin J, Wang ZH, Chai WX et al (2017) Fabrication of inner grooved hollow fiber membranes using microstructured spinneret for nerve regeneration. J Manuf Sci Eng 139(11):111007. https://doi.org/10.1115/1.4037430
48. Adidharma W, Wang Y, Kotsis SV et al (2024) Utilization trends of nerve autograft alternatives for the reconstruction of peripheral nerve defects. Plast Reconstr Surg 153(4):863–872.

https://doi.org/10.1097/PRS.0000000000011153
49. Leckenby JI, Furrer C, Haug L et al (2020) A retrospective case series reporting the outcomes of Avance nerve allografts in the treatment of peripheral nerve injuries. Plast Reconstr Surg 145(2): 368e–381e. https://doi.org/10.1097/PRS.0000000000006485
50. Safa B, Buncke G (2016) Autograft substitutes. Hand Clinics 32(2):127–140. https://doi.org/10.1016/j.hcl.2015.12.012
51. Ansaripour A, Thompson A, Styron JF et al (2024) Cost-effectiveness analysis of Avance® allograft for the treatment of peripheral nerve injuries in the USA. J Comp Eff Res 13(1): e230113. https://doi.org/10.57264/cer-2023-0113
52. Rao ZL, Lin ZD, Song PP et al (2022) Biomaterial-based Schwann cell transplantation and Schwann cell-derived biomaterials for nerve regeneration. Front Cell Neurosci 16:926222. https://doi.org/10.3389/fncel.2022.926222
53. Nave KA, Werner HB (2014) Myelination of the nervous system: mechanisms and functions. Annu Rev Cell Dev Biol 30(1): 503–533. https://doi.org/10.1146/annurev-cellbio-100913-013101
54. Nocera G, Jacob C (2020) Mechanisms of Schwann cell plasticity involved in peripheral nerve repair after injury. Cell Mol Life Sci 77(20):3977–3989. https://doi.org/10.1007/s00018-020-03516-9
55. Kang Y, Liu YT, Liu ZY et al (2019) Differentiated human adipose-derived stromal cells exhibit the phenotypic and functional characteristics of mature Schwann cells through a modified approach. Cytotherapy 21(9):987–1003. https://doi.org/10.1016/j.jcyt.2019.04.061
56. Moss KR, Mi R, Kawaguchi R et al (2024) hESC- and hiPSC-derived Schwann cells are molecularly comparable and functionally equivalent. iScience 27(6):109855. https://doi.org/10.1016/j.isci.2024.109855
57. Xu YH, Kim CS, Saylor DM et al (2017) Polymer degradation and drug delivery in PLGA-based drug-polymer applications: a review of experiments and theories. J Biomed Mater Res B Appl Biomater 105(6):1692–1716. https://doi.org/10.1002/jbm.b.33648
58. Deval E, Noël J, Lay N et al (2008) ASIC3, a sensor of acidic and primary inflammatory pain. EMBO J 27(22):3047–3055. https://doi.org/10.1038/emboj.2008.213
59. Luis AL, Rodrigues JM, Amado S et al (2007) PLGA 90/10 and caprolactone biodegradable nerve guides for the reconstruction of the rat sciatic nerve. Microsurgery 27(2):125–137. https://doi.org/10.1002/micr.20317
60. Kehoe S, Zhang XF, Boyd D (2012) FDA approved guidance conduits and wraps for peripheral nerve injury: a review of materials and efficacy. Injury 43(5):553–572. https://doi.org/10.1016/j.injury.2010.12.030
61. Lin DX, Luo CC, Wei PY et al (2024) YAP1 recognizes inflammatory and mechanical cues to exacerbate benign prostatic hyperplasia via promoting cell survival and fibrosis. Adv Sci 11(5): e2304274. https://doi.org/10.1002/advs.202304274
62. Xu HX, Yan YH, Li SP (2011) PDLLA/chondroitin sulfate/chitosan/NGF conduits for peripheral nerve regeneration. Biomaterials 32(20):4506–4516. https://doi.org/10.1016/j.biomaterials.2011.02.023
63. Angius D, Wang H, Spinner RJ et al (2012) A systematic review of animal models used to study nerve regeneration in tissue-engineered scaffolds. Biomaterials 33(32):8034–8039. https://doi.org/10.1016/j.biomaterials.2012.07.056
64. Kaplan HM, Mishra P, Kohn J (2015) The overwhelming use of rat models in nerve regeneration research may compromise designs of nerve guidance conduits for humans. J Mater Sci Mater Med 26(8):226. https://doi.org/10.1007/s10856-015-5558-4
65. Schuh CM, Hercher D, Stainer M et al (2016) Extracorporeal shockwave treatment: a novel tool to improve Schwann cell isolation and culture. Cytotherapy 18(6):760–770. https://doi.org/10.1016/j.jcyt.2016.03.002
66. Fuentes-Flores A, Geronimo-Olvera C, Girardi K et al (2023) Senescent Schwann cells induced by aging and chronic denervation impair axonal regeneration following peripheral nerve injury. EMBO Mol Med 15(12):e17907. https://doi.org/10.15252/emmm.202317907